

# UC Santa Cruz

## UC Santa Cruz Previously Published Works

**Title**

Conformational Flexibility in Respiratory Syncytial Virus G Neutralizing Epitopes.

**Permalink**

<https://escholarship.org/uc/item/2z2100j8>

**Journal**

Journal of virology, 94(6)

**ISSN**

0022-538X

**Authors**

Fedechkin, Stanislav O  
George, Natasha L  
Nuñez Castrejon, Ana M  
et al.

**Publication Date**

2020-02-01

**DOI**

10.1128/jvi.01879-19

Peer reviewed



## ABSTRACT

Respiratory syncytial virus (RSV) is a top cause of severe lower respiratory tract disease and mortality in infants and the elderly. Currently, no vaccine or effective treatment exists for RSV. The RSV G glycoprotein mediates viral attachment to cells and contributes to pathogenesis by modulating host immunity through interactions with the human chemokine receptor CX3CR1. Antibodies targeting the RSV G central conserved domain are protective in both prophylactic and post-infection animal models. Here we describe the crystal structure of the broadly-neutralizing human monoclonal antibody 3G12 bound to the RSV G central conserved domain. Antibody 3G12 binds to a conformational epitope composed of highly conserved residues, explaining its broad neutralization activity. Surprisingly, RSV G complexed with 3G12 adopts a distinct conformation not observed in previously described RSV G–antibody structures. Comparison to other structures reveals that the RSV G central conserved domain is flexible and can adopt multiple conformations in the regions flanking the cysteine noose. We also show that restriction of RSV G flexibility with a proline mutation abolishes binding to antibody 3G12 but not antibody 3D3, which recognizes a different conformation of RSV G. Our studies provide new insights for rational vaccine design, indicating the importance of preserving both the global structural integrity of antigens and local conformational flexibility at antigenic sites, which may elicit a more diverse antibody response and broader protection against infection and disease.

40 **IMPORTANCE**

41 Respiratory syncytial virus (RSV) causes severe respiratory infections in infants, young  
42 children, and the elderly, and currently no licensed vaccine exists. In this study, we  
43 describe the crystal structure of the RSV surface glycoprotein G in complex with a  
44 broadly-neutralizing human monoclonal antibody. The antibody binds to RSV G at a  
45 highly conserved region stabilized by two disulfide bonds, but it captures RSV G in a  
46 conformation not previously observed, revealing that this region is both structured and  
47 flexible. Importantly, our findings provide insight for the design of vaccines that elicit  
48 diverse antibodies, which may provide broad protection from infection and disease.

## INTRODUCTION

Respiratory syncytial virus (RSV) is a globally prevalent virus that affects the airways and lungs. Infants and young children are at the highest risk of severe outcome from RSV infection, with 33.1 million episodes of lower respiratory tract infection and approximately 3.2 million hospital visits and 118,200 deaths per year worldwide in children under age 5 due to RSV (1). RSV is also a major cause of illness in adults older than 65 years and immunocompromised individuals, with an estimated 14,000 deaths per year in the United States (2). Hospitalization due to RSV is a major economic burden, especially in preterm infants and older adults (3).

Currently, no licensed vaccine exists for the prevention of RSV infection, making RSV one of the highest burden diseases with no readily available preventative measure. The only FDA-approved therapy for RSV is passive prophylaxis with palivizumab (Synagis), a monoclonal antibody, which reduces disease severity and hospitalization (4). Palivizumab's approved use is limited to high-risk premature birth infants; moreover, the high cost, approximately \$10,000, for a full course of therapy, limits use even in that narrow indication (5). The need for widely available vaccines and therapies for RSV is evidenced from the 19 vaccine candidates and therapeutic monoclonal antibodies in clinical trials (6).

RSV is a negative-sense single stranded RNA virus with two major glycoproteins on the virion surface: the attachment glycoprotein (G) and the fusion glycoprotein (F) (7). RSV G is responsible for cellular attachment to host cells and RSV F causes the viral membrane to fuse with the target host cell membrane. While both RSV F and G are immunogenic and are targeted by neutralizing antibodies, the majority of neutralizing

antibodies in human sera target RSV F (8, 9). As such, most RSV vaccine candidates and therapeutic antibodies currently in development focus on RSV F. However, RSV that does not express the G protein is highly attenuated *in vivo* (10), and monoclonal antibodies that target RSV G are protective *in vivo* (11-21). In humans, anti-G antibodies are associated with lower clinical disease severity scores, despite an abundance in sera more than 30 times lower than anti-F antibodies (8). Thus, the RSV G protein is increasingly recognized as an important target for RSV vaccine and therapeutic antibody development (22).

RSV G is a type II membrane protein containing two mucin-like regions coated with 30-40 O-linked glycans and 3-5 N-linked glycans (Fig. 1A) (7, 23, 24). There are two forms of RSV G produced during infection. Membrane-bound RSV G is responsible for virus attachment to airway epithelial cells via the human chemokine receptor CX3CR1 (25-28). A secreted form of RSV G, derived from a second translation initiation site at Met48 and released from the membrane by proteolysis, is expressed early in infection (first ~6 hours, prior to the release of virions at ~12 hours) (Fig. 1A) (29). Secreted RSV G modulates signaling and trafficking of CX3CR1<sup>+</sup> immune cells, contributing to airway congestion and pathogenesis (26, 27, 30-33). Between the two mucin-like regions of RSV G is a central conserved domain (CCD) of ~40 highly conserved amino acids, including four invariant cysteines forming a cysteine noose motif with two disulfide bonds (1-4, 2-3 connectivity) (Fig. 1A) (34-36). While the C-terminus of the RSV G CCD possesses a heparin binding domain (Fig. 1A) (37, 38), initial RSV infection is thought to be mediated primarily by interaction between the RSV G CCD and

CX3CR1 on ciliated airway cells (25-28), which do not have measurable heparan sulfate proteoglycans on their surfaces (39).

Broadly neutralizing monoclonal antibodies (bnmAbs) that target RSV G are able to neutralize RSV infectivity in cell culture, including in HAE cells, and significantly reduce RSV viral loads and disease in both prophylactic and post-infection animal models (12, 14-16, 21, 25, 28, 40, 41). In addition, treatment with anti-RSV G mAbs reduces BAL cell influx including RSV G protein-induced leukocyte migration and eosinophilic inflammatory response, resulting in decreased airway congestion (15, 33, 42). Anti-G mAbs have also been shown to reduce mucus production and to restore beneficial antiviral IFN- $\alpha$  (18, 42-44). Most of the anti-G bnmAbs that have been studied to date bind with high affinity to RSV G ( $K_D$  (dissociation constant) = 1.1 pM - 3.3 nM) and bind to linear epitopes within the RSV G CCD as determined by linear epitope mapping techniques (17, 21, 40, 45). Recently, two studies elucidated four high-resolution crystal structures of antibody-RSV G CCD complexes (16, 46). Unexpectedly, all four antibodies have additional interactions outside their linear epitopes, revealing a previously unappreciated role of the disulfide-stabilized cysteine noose in forming conformational epitopes and contributing to high-affinity antibody binding.

Here we investigated the human bnmAb 3G12, which reduces viral loads, airway hyper-responsiveness, and inflammation in both prophylactic and post-infection mouse models of RSV infection (12, 21). Linear epitope mapping experiments have shown that bnmAb 3G12 binds to RSV G CCD residues 167-176, which is shifted downstream compared to other anti-G bnmAbs in the panel that bind primarily RSV G residues 162-169 (12, 21). We hypothesized that structural studies into the 3G12 epitope might reveal

117 additional information about the mechanisms of high-affinity antibody binding and broad  
118 neutralization against RSV A and B strains. We present here the structure of antibody  
119 3G12 bound to the RSV G CCD, which reveals a novel conformational epitope composed  
120 of highly conserved residues. Comparison to other structures highlights the flexible  
121 nature of the RSV G CCD. We further show that RSV G flexibility is important for  
122 binding by antibody 3G12. Overall, these studies have broad implications for vaccine  
123 antigen design. The studies highlight the importance of preserving antigen structural  
124 integrity and also maintaining flexibility in antigenic sites, in order to elicit a diverse  
125 antibody response.

## 127 **RESULTS**

### 128 **Fab 3G12-RSV G<sup>157-197</sup> complex structure**

129 We investigated bnmAb 3G12, a native human antibody that binds RSV G with  
130 high affinity,  $K_D = 579$  pM. Antibody 3G12 shows broadly neutralizing activity across  
131 diverse lab and clinical RSV strains (21). To understand the molecular basis for the broad  
132 reactivity of bnmAb 3G12 and to determine if it binds to a larger conformational epitope  
133 beyond that predicted by linear epitope mapping, we used X-ray crystallographic studies  
134 to determine the structure of bnmAb 3G12 bound to the RSV G CCD (Fig. 1A). Purified  
135 antigen-binding fragment (Fab) 3G12 was mixed with recombinant RSV G<sup>157-197</sup>, which  
136 formed a stable complex in solution. We crystallized the Fab 3G12-RSV G<sup>157-197</sup> complex  
137 and determined its crystal structure to 2.9 Å resolution (Fig. 1B, Fig. 1C, and Table 1).

138 The Fab 3G12-RSV G<sup>157-197</sup> complex structure reveals a 924 Å<sup>2</sup> epitope on the  
139 RSV G CCD, with 3G12 heavy chain burying 697 Å<sup>2</sup> and the light chain burying 227 Å<sup>2</sup>



of the epitope (Fig. 1B). Similar to RSV G-antibody structures determined previously (16, 46), antibody 3G12 binds to a *conformational epitope* comprising RSV G residues 160-179, 182 and 189, revealing additional interactions beyond the linear epitope residues 167-176 (Fig. 1). Epitope residues are invariant or highly conserved (Fig. 1A), explaining the broad reactivity of bnmAb 3G12 for diverse RSV strains. The 3G12 heavy chain complementarity-determining regions (HCDRs) account for the majority of the interactions and buried surface with the RSV G CCD, with the HCDR2 burying the largest portion with 315 Å<sup>2</sup> and HCDR3 accounting for 284 Å<sup>2</sup> (Fig. 1C). On the light chain complementarity-determining regions (LCDRs), LCDR3 buries 169.5 Å<sup>2</sup> on the N-terminal end of the RSV G CCD, while LCDR1 and the Fab 3G12 N-terminal residues form additional minor interactions (Fig. 1C). The 3G12 heavy chain CDR2 stabilizes residues 167-170 of RSV G by several hydrogen bonds and van der Waals interactions (Fig. 1C). In addition, residues from all three of the HCDRs from bnmAb 3G12 stabilize hydrophobic interactions with RSV G residues F163, F165, F168, F170, P172, and I175, forming a hydrophobic core-like region within the antibody 3G12-RSV G complex (Fig. 1C). Interestingly, the helix on the C-terminal end of the cysteine noose, which encompasses the CX3C motif (residues 180-186), has almost no interactions with antibody 3G12, unlike other antibody-RSV G CCD structures where this helix has a role in antibody binding (Fig. 1C and Fig. 2).

## **RSV G CCD epitopes and conformational flexibility**

To better understand the conformational flexibility in the RSV G CCD, all known structures of the CCD bound by antibodies were compared (Fig. 2). The structures were

aligned at the cysteine noose region (~ residues 170-187), which has an RMSD of  $<0.6 \text{ \AA}$  across all structures. The region N-terminal to the cysteine noose (~ residues 160-169) adopts a different conformation in each structure (RMSD of  $3\text{-}5 \text{ \AA}$ ) and varies in secondary structural elements (i.e. forms a helix when bound to antibody 3D3 and forms a strand when bound to antibody CB002.5)(Fig. 2). RSV G residue N169 appears to be flexible across all of the structures and may be one of the last ordered residues in the N-terminal region of the CCD. Similarly, the C-terminal region after K187 may be flexible and capable of adopting multiple conformations (Fig. 2). These C-terminal non-interacting RSV G CCD residues are present in most of the complexes but do not have visible electron density, suggesting that they are dynamic and flexible. Overall, the RSV G CCD cysteine noose is structurally conserved and is an important structural element for antibody binding, however the N- and C-terminal regions of the CCD are flexible and are captured in different conformations by diverse antibodies.

### **Role of RSV G flexibility in bnmAb binding**

To evaluate the role of RSV G flexibility in bnmAb binding, we sought to investigate a mutant of RSV G with restricted flexibility in its CCD. We chose the mutant F170P, which was previously identified in neutralization escape mutants of respiratory syncytial virus grown in the presence of an anti-G monoclonal antibody (47). The F170 side chain contributes only 1.3% of the 3G12 epitope ( $12 \text{ \AA}^2$  of the  $924 \text{ \AA}^2$ ), suggesting that mutation of the side chain alone would not substantially affect bnmAb 3G12 binding. However, when bound to bnmAb 3G12, RSV G residue F170 has a Phi torsion angle of  $-143$  degrees, whereas a typical proline is restricted to a Phi torsion angle of  $-60$  degrees.

Thus, we reasoned that the proline mutation would restrict the flexibility of the RSV G CCD and could affect bnmAb binding. We produced and purified the wild-type RSV G ectodomain (RSV G<sup>ecto</sup>) and its mutant (RSV G<sup>ecto</sup> F170P) (Fig. 3A). We then evaluated binding by bnmAbs 3G12 and 3D3, which bind to two very different conformations of the RSV G CCD (Fig. 3B). Biolayer interferometry binding studies reveal that while both bnmAbs bind to wild-type RSV G<sup>ecto</sup> with high-affinity, bnmAb 3G12, but not 3D3, completely lost binding to the mutant RSV G<sup>ecto</sup> F170P (Fig. 3C and Table 2). These data reveal that the mutant RSV G<sup>ecto</sup> F170P can adopt the conformation for the 3D3 epitope, however it cannot adopt the conformation for the 3G12 epitope.

## DISCUSSION

Our study highlights how even disulfide constrained antigens can have flexible, dynamic antigenic sites, and that different high-affinity antibodies can target these sites in distinct ways. We describe the crystal structure of the human bnmAb 3G12 bound to the RSV G CCD and show that bnmAb 3G12 binding is dependent on RSV G flexibility. The antibody binds to a conformational epitope composed of highly conserved residues, explaining its broad reactivity to diverse strains of RSV. The antibody interacts mainly with the RSV G CCD's N-terminal region, in a conformation distinct from all other known CCD structures, suggesting that the RSV G CCD is flexible outside of its rigid disulfide bonded cysteine noose region. Residue N169 likely represents a 'hinge' residue, where the N-terminal region of the CCD preceding N169 appears to be flexible and capable of adopting multiple conformations and even secondary structures. Likewise, residues after K187 in the C-terminal region of the CCD also appear to be flexible. Thus,

RSV G is part of a growing list of antigens with flexible or intrinsically disordered regions (IDRs) that are targeted by antibodies (48-56).

The observation of different conformations of RSV G CCD raises several important questions. Does RSV G move freely and randomly, and do our structures reveal momentary snapshots captured by antibody binding? What conformation does RSV G adopt when interacting with the human CX3CR1 receptor? We note that none of the conformations have any substantial tertiary structure stabilizing interactions within the CCD or clearly defined secondary structure. Therefore it is unlikely that RSV G assumes distinct conformations without additional external stabilizing interactions. One form of stabilization may come from the oligomerization state of RSV G. It has been previously suggested that RSV G exists as a trimer or tetramer (57, 58). The extensive glycosylation of RSV G in the mucin-like regions flanking the CCD may also restrict RSV G flexibility. It is also possible that RSV G interacts with RSV F on the virus surface, creating a quaternary structure that may limit RSV G to the defined structures like those captured by the antibodies discussed in this paper. Interestingly, in a RSV virus-like particle vaccine containing F and G, the conformation of F affected the immunogenicity of G (59). These factors may be important in the design of an RSV vaccine.

Our study also has important implications for vaccine antigen design in a broader sense. Recently, there has been a trend to stabilize antigens based on structural analyses to elicit higher levels of neutralizing antibodies targeting specific epitopes, e.g. HIV gp120, influenza hemagglutinin, MERS-Coronavirus spike, human parainfluenza virus fusion protein, human metapneumovirus fusion protein, and RSV fusion protein (60-71).

A common approach to antigen stabilization in many of the aforementioned studies involves the introduction of proline substitutions and disulfide bonds, which can stabilize by limiting polypeptide backbone mobility. However, antigen over-stabilization could limit the *diversity* of antibody responses. In support of this concept, we show that limiting flexibility of RSV G with a proline mutation abolishes the epitope for the high-affinity bnmAb 3G12. Thus, when designing stabilized antigens that display specific epitopes, one should also consider the benefits of preserving the native flexibility of antigenic sites, which may elicit a more diverse immune response and may offer better protection against virus escape (Fig. 4). Incorporating antibody repertoire analysis technologies during vaccine development could provide opportunities to evaluate antibody diversity that is elicited by stabilized antigens.

## MATERIALS AND METHODS

**Production of bnmAb 3G12 and Fab 3G12.** Recombinant bnmAb 3G12 was produced by transient-transfection in CHO cells and purification by immobilized protein A, as described previously (21, 45). Fab 3G12 was generated by incubation of bnmAb 3G12 with immobilized papain, followed by removal of the Fc fragment with immobilized protein A. Fab 3G12 was then purified by Superdex 200 size-exclusion chromatography in 10 mM Tris-HCl pH 8.0 and 150 mM NaCl.

**Expression and purification of RSV G<sup>157-197</sup>.** A synthetic gene codon-optimized for *E. coli* encoding RSV G (strain A2) amino acids 157 to 197 (UniProtKB entry P03423) with a C-terminal 6× histidine purification tag was cloned into pET52b. Recombinant RSV

G<sup>157-197</sup> was expressed overnight in *E. coli* BL21(DE3) at 18°C. *E. coli* cells were lysed by ultrasonication in 20 mM Tris-HCl (pH 8.0), 150 mM NaCl, and 25 mM imidazole (buffer A) containing 2 µM MgCl<sub>2</sub>, benzonase, and protease inhibitors. RSV G<sup>157-197</sup> was purified from soluble lysates by HisTrap FF affinity chromatography and eluted with a gradient into buffer B (buffer A containing 500 mM imidazole).

#### **Formation and structure determination of the Fab 3G12-RSV G<sup>157-197</sup> complex.**

Purified RSV G<sup>157-197</sup> was mixed in 2-molar excess with purified Fab 3G12, incubated for 1 hour at 4° C, and purified by Superdex 75 size-exclusion chromatography in 10 mM Tris-HCl pH 8.0 and 150 mM NaCl. The Fab 3G12-RSV G<sup>157-197</sup> complex was concentrated to 15 mg/ml. Crystals were grown by hanging drop vapor diffusion at 22°C with a well solution of 1.8 M Ammonium Sulfate and 100 mM Sodium acetate trihydrate (pH 4.4). Crystals were transferred into a cryoprotectant solution of 2.0 M Ammonium Sulfate, 100 mM Sodium acetate trihydrate (pH 4.4) and 25% glycerol and flash-frozen in liquid nitrogen. Diffraction data were collected at cryogenic temperature at the Advanced Light Source on beamline 8.3.1 using a wavelength of 1.11503 Å. Diffraction data from a single crystal were processed with iMosflm (72) and Aimless (73) (Table 1). The Fab 3G12-RSV G<sup>157-197</sup> complex structure was solved by molecular replacement with the Fab from PDB 5K59 and the program PHASER (74), and the structure was refined and manually rebuilt using PHENIX (75) and Coot (76), respectively (Table 1).

**Expression and purification of RSV G<sup>ecto</sup> and RSV G<sup>ecto</sup> F170P.** A codon-optimized synthetic gene encoding RSV G (strain A2) amino acids 64 to 298 (UniProtKB entry

P03423) was cloned into pCF in-frame with an N-terminal CCR5 signal sequence and C-terminal His-tag and Twin-Strep purification tags. The F170P mutation was introduced by Phusion site-directed mutagenesis and verified by Sanger sequencing. Recombinant RSV G<sup>ecto</sup> and RSV G<sup>ecto</sup> F170P were produced by transient-transfection in HEK293F cells with Effectene Transfection Reagent (Qiagen). After 5 days, cell media was supplemented with BioLock (IBA) and 20 mM Tris-HCl pH 8.0 and 0.22µm-filtered. RSV G<sup>ecto</sup> and RSV G<sup>ecto</sup> F170P were batch purified from media with Strep-Tactin resin (IBA), washed, and eluted with Strep-Tactin elution buffer (50 mM Tris pH 8.0, 150mM NaCl, 1mM EDTA, 2.5mM desthiobiotin). RSV G<sup>ecto</sup> and RSV G<sup>ecto</sup> F170P were concentrated and dialyzed into PBS using 10 kDa spin concentrators. Protein purity was evaluated by SDS-polyacrylamide gel electrophoresis.

**Binding affinity analyses.** An Octet RED96e biolayer interferometry instrument was used to evaluate binding of bnmAbs 3G12 and 3D3 to RSV G<sup>ecto</sup> and RSV G<sup>ecto</sup> F170P. Antibody 3G12 or 3D3 at 1 µg/ml in Octet buffer (phosphate buffered saline pH 7.4, 0.05% Tween-20, 1% BSA) was loaded onto Anti-Human IgG Fc Capture (AHC) biosensors, and two-fold serially diluted RSV G<sup>ecto</sup> or RSV G<sup>ecto</sup> F170P, from 40 nM to 0.625 nM, was assessed for binding. Red lines are the fit of a global association and dissociation with a 1:1 model, with at least 5 curves used to determine binding on- and off-rates and to calculate dissociation constants.

**Accession code.** Coordinates and structure factors have been deposited in the Protein Data Bank under accession code 6UVO.

**ACKNOWLEDGMENTS**

We thank Dr. Sarvind Tripathi for assistance in crystallographic data collection. We thank Dr. Edgar Tenorio for reviewing the manuscript. R.M.D. is supported by the National Institute of Allergy and Infectious Diseases (NIAID) grants R21AI130605 and R56AI141537. L.M.K. acknowledges partial support from NIAID grant 5R44AI122360-02. This research used resources of the Advanced Light Source (ALS), which is a U.S. Department of Energy (DOE) Office of Science User Facility under contract no. DE-AC02-05CH11231. Beamline 8.3.1 at the Advanced Light Source is operated by the University of California Office of the President, Multicampus Research Programs and Initiatives grant MR-15-328599, the National Institutes of Health (R01 GM124149 and P30 GM124169), Plexxikon Inc.



## REFERENCES

1. **Shi T, McAllister DA, O'Brien KL, Simoes EAF, Madhi SA, Gessner BD, Polack FP, Balsells E, Acacio S, Aguayo C, Alassani I, Ali A, Antonio M, Awasthi S, Awori JO, Azziz-Baumgartner E, Baggett HC, Baillie VL, Balmaseda A, Barahona A, Basnet S, Bassat Q, Basualdo W, Bigogo G, Bont L, Breiman RF, Brooks WA, Broor S, Bruce N, Bruden D, Buchy P, Campbell S, Carosone-Link P, Chadha M, Chipeta J, Chou M, Clara W, Cohen C, de Cuellar E, Dang DA, Dash-Yandag B, Deloria-Knoll M, Dherani M, Eap T, Ebruke BE, Echavarria M, de Freitas Lazaro Emediato CC, Fasce RA, Feikin DR, Feng L, et al.** 2017. Global, regional, and national disease burden estimates of acute lower respiratory infections due to respiratory syncytial virus in young children in 2015: a systematic review and modelling study. *Lancet* **390**:946-958.
2. **Falsey AR, Hennessey PA, Formica MA, Cox C, Walsh EE.** 2005. Respiratory syncytial virus infection in elderly and high-risk adults. *N Engl J Med* **352**:1749-1759.
3. **Amand C, Tong S, Kieffer A, Kyaw MH.** 2018. Healthcare resource use and economic burden attributable to respiratory syncytial virus in the United States: a claims database analysis. *BMC Health Services Research* **18**:294.
4. **Anonymous.** 1998. Palivizumab, a Humanized Respiratory Syncytial Virus Monoclonal Antibody, Reduces Hospitalization From Respiratory Syncytial Virus Infection in High-risk Infants. *Pediatrics* **102**:531-537.
5. **Meissner HC, Kimberlin DW.** 2013. RSV immunoprophylaxis: does the benefit justify the cost? *Pediatrics* **132**:915-918.
6. **Mazur NI, Higgins D, Nunes MC, Melero JA, Langedijk AC, Horsley N, Buchholz UJ, Openshaw PJ, McLellan JS, Englund JA, Mejias A, Karron RA, Simoes EA, Knezevic I, Ramilo O, Piedra PA, Chu HY, Falsey AR, Nair H, Kragten-Tabatabaie L, Greenough A, Baraldi E, Papadopoulos NG, Vekemans J, Polack FP, Powell M, Satav A, Walsh EE, Stein RT, Graham BS, Bont LJ, Respiratory Syncytial Virus Network F.** 2018. The respiratory syncytial virus vaccine landscape: lessons from the graveyard and promising candidates. *Lancet Infect Dis* **18**:e295-e311.
7. **McLellan JS, Ray WC, Peeples ME.** 2013. Structure and function of respiratory syncytial virus surface glycoproteins. *Curr Top Microbiol Immunol* **372**:83-104.
8. **Capella C, Chaiwatpongsakorn S, Gorrell E, Risch ZA, Ye F, Mertz SE, Johnson SM, Moore-Clingenpeel M, Ramilo O, Mejias A, Peeples ME.** 2017. Prefusion F, postfusion F, G antibodies and disease severity in infants and young children with acute respiratory syncytial virus infection. *J Infect Dis* doi:10.1093/infdis/jix489.
9. **Ngwuta JO, Chen M, Modjarrad K, Joyce MG, Kanekiyo M, Kumar A, Yassine HM, Moin SM, Killikelly AM, Chuang GY, Druz A, Georgiev IS, Rundlet EJ, Sastry M, Stewart-Jones GB, Yang Y, Zhang B, Nason MC, Capella C, Peeples ME, Ledgerwood JE, McLellan JS, Kwong PD, Graham BS.** 2015. Prefusion F-specific antibodies determine the magnitude of RSV neutralizing activity in human sera. *Sci Transl Med* **7**:309ra162.
10. **Teng MN, Whitehead SS, Collins PL.** 2001. Contribution of the respiratory syncytial virus G glycoprotein and its secreted and membrane-bound forms to virus replication in vitro and in vivo. *Virology* **289**:283-296.
11. **Techaarpornkul S, Barretto N, Peeples ME.** 2001. Functional analysis of recombinant respiratory syncytial virus deletion mutants lacking the small hydrophobic and/or attachment glycoprotein gene. *J Virol* **75**:6825-6834.
12. **Han J, Takeda K, Wang M, Zeng W, Jia Y, Shiraishi Y, Okamoto M, Dakhama A, Gelfand EW.** 2014. Effects of anti-g and anti-f antibodies on airway function after respiratory syncytial virus infection. *Am J Respir Cell Mol Biol* **51**:143-154.
13. **Boyoglu-Barnum S, Todd SO, Chirkova T, Barnum TR, Gaston KA, Haynes LM, Tripp RA, Moore ML, Anderson LJ.** 2015. An anti-G protein monoclonal antibody treats RSV disease more effectively than an anti-F monoclonal antibody in BALB/c mice. *Virology* **483**:117-125.
14. **Boyoglu-Barnum S, Chirkova T, Todd SO, Barnum TR, Gaston KA, Jorquera P, Haynes LM, Tripp RA, Moore ML, Anderson LJ.** 2014. Prophylaxis with a respiratory syncytial virus (RSV) anti-G protein monoclonal antibody shifts the adaptive immune response to RSV rA2-line19F infection from Th2 to Th1 in BALB/c mice. *J Virol* **88**:10569-10583.

368 15. **Boyoglu-Barnum S, Gaston KA, Todd SO, Boyoglu C, Chirkova T, Barnum TR, Jorquera P,**  
369 **Haynes LM, Tripp RA, Moore ML, Anderson LJ.** 2013. A respiratory syncytial virus (RSV)  
370 anti-G protein F(ab')<sub>2</sub> monoclonal antibody suppresses mucous production and breathing effort in  
371 RSV rA2-line19F-infected BALB/c mice. *J Virol* **87**:10955-10967.

372 16. **Jones HG, Ritschel T, Pascual G, Brakenhoff JPJ, Keogh E, Furmanova-Hollenstein P,**  
373 **Lanckacker E, Wadia JS, Gilman MSA, Williamson RA, Roymans D, van 't Wout AB,**  
374 **Langedijk JP, McLellan JS.** 2018. Structural basis for recognition of the central conserved  
375 region of RSV G by neutralizing human antibodies. *PLoS Pathog* **14**:e1006935.

376 17. **Lee HJ, Lee JY, Park MH, Kim JY, Chang J.** 2017. Monoclonal Antibody against G  
377 Glycoprotein Increases Respiratory Syncytial Virus Clearance In Vivo and Prevents Vaccine-  
378 Enhanced Diseases. *PLoS One* **12**:e0169139.

379 18. **Miao C, Radu GU, Caidi H, Tripp RA, Anderson LJ, Haynes LM.** 2009. Treatment with  
380 respiratory syncytial virus G glycoprotein monoclonal antibody or F(ab')<sub>2</sub> components mediates  
381 reduced pulmonary inflammation in mice. *J Gen Virol* **90**:1119-1123.

382 19. **Radu GU, Caidi H, Miao C, Tripp RA, Anderson LJ, Haynes LM.** 2010. Prophylactic  
383 treatment with a G glycoprotein monoclonal antibody reduces pulmonary inflammation in  
384 respiratory syncytial virus (RSV)-challenged naive and formalin-inactivated RSV-immunized  
385 BALB/c mice. *J Virol* **84**:9632-9636.

386 20. **Caidi H, Harcourt JL, Tripp RA, Anderson LJ, Haynes LM.** 2012. Combination therapy using  
387 monoclonal antibodies against respiratory syncytial virus (RSV) G glycoprotein protects from  
388 RSV disease in BALB/c mice. *PLoS One* **7**:e51485.

389 21. **Collarini EJ, Lee FE, Foord O, Park M, Sperinde G, Wu H, Harriman WD, Carroll SF,**  
390 **Ellsworth SL, Anderson LJ, Tripp RA, Walsh EE, Keyt BA, Kauvar LM.** 2009. Potent high-  
391 affinity antibodies for treatment and prophylaxis of respiratory syncytial virus derived from B  
392 cells of infected patients. *J Immunol* **183**:6338-6345.

393 22. **Tripp RA, Power UF, Openshaw PJM, Kauvar LM.** 2018. Respiratory Syncytial Virus:  
394 Targeting the G Protein Provides a New Approach for an Old Problem. *J Virol* **92**.

395 23. **Satake M, Coligan JE, Elango N, Norrby E, Venkatesan S.** 1985. Respiratory syncytial virus  
396 envelope glycoprotein (G) has a novel structure. *Nucleic Acids Res* **13**:7795-7812.

397 24. **Wertz GW, Collins PL, Huang Y, Gruber C, Levine S, Ball LA.** 1985. Nucleotide sequence of  
398 the G protein gene of human respiratory syncytial virus reveals an unusual type of viral membrane  
399 protein. *Proc Natl Acad Sci U S A* **82**:4075-4079.

400 25. **Johnson SM, McNally BA, Ioannidis I, Flano E, Teng MN, Oomens AG, Walsh EE, Peeples**  
401 **ME.** 2015. Respiratory Syncytial Virus Uses CX3CR1 as a Receptor on Primary Human Airway  
402 Epithelial Cultures. *PLoS Pathog* **11**:e1005318.

403 26. **Tripp RA, Jones LP, Haynes LM, Zheng H, Murphy PM, Anderson LJ.** 2001. CX3C  
404 chemokine mimicry by respiratory syncytial virus G glycoprotein. *Nat Immunol* **2**:732-738.

405 27. **Chirkova T, Lin S, Oomens AG, Gaston KA, Boyoglu-Barnum S, Meng J, Stobart CC,**  
406 **Cotton CU, Hartert TV, Moore ML, Ziady AG, Anderson LJ.** 2015. CX3CR1 is an important  
407 surface molecule for respiratory syncytial virus infection in human airway epithelial cells. *J Gen*  
408 *Virol* **96**:2543-2556.

409 28. **Jeong KI, Piepenhagen PA, Kishko M, DiNapoli JM, Groppo RP, Zhang L, Almond J,**  
410 **Kleanthous H, Delagrave S, Parrington M.** 2015. CX3CR1 Is Expressed in Differentiated  
411 Human Ciliated Airway Cells and Co-Localizes with Respiratory Syncytial Virus on Cilia in a G  
412 Protein-Dependent Manner. *PLoS One* **10**:e0130517.

413 29. **Bukreyev A, Yang L, Fricke J, Cheng L, Ward JM, Murphy BR, Collins PL.** 2008. The  
414 secreted form of respiratory syncytial virus G glycoprotein helps the virus evade antibody-  
415 mediated restriction of replication by acting as an antigen decoy and through effects on Fc  
416 receptor-bearing leukocytes. *J Virol* **82**:12191-12204.

417 30. **Chirkova T, Boyoglu-Barnum S, Gaston KA, Malik FM, Trau SP, Oomens AG, Anderson**  
418 **LJ.** 2013. Respiratory syncytial virus G protein CX3C motif impairs human airway epithelial and  
419 immune cell responses. *J Virol* **87**:13466-13479.

420 31. **Harcourt J, Alvarez R, Jones LP, Henderson C, Anderson LJ, Tripp RA.** 2006. Respiratory  
421 syncytial virus G protein and G protein CX3C motif adversely affect CX3CR1+ T cell responses.  
422 *J Immunol* **176**:1600-1608.

423 32. **Arnold R, Konig B, Werchau H, Konig W.** 2004. Respiratory syncytial virus deficient in soluble  
424 G protein induced an increased proinflammatory response in human lung epithelial cells. *Virology*  
425 **330**:384-397.

426 33. **Haynes LM, Jones LP, Barskey A, Anderson LJ, Tripp RA.** 2003. Enhanced disease and  
427 pulmonary eosinophilia associated with formalin-inactivated respiratory syncytial virus  
428 vaccination are linked to G glycoprotein CX3C-CX3CR1 interaction and expression of substance  
429 P. *J Virol* **77**:9831-9844.

430 34. **Sugawara M, Czaplicki J, Ferrage J, Haeuw JF, Power UF, Corvaia N, Nguyen T, Beck A,**  
431 **Milton A.** 2002. Structure-antigenicity relationship studies of the central conserved region of  
432 human respiratory syncytial virus protein G. *J Pept Res* **60**:271-282.

433 35. **Langedijk JP, de Groot BL, Berendsen HJ, van Oirschot JT.** 1998. Structural homology of the  
434 central conserved region of the attachment protein G of respiratory syncytial virus with the fourth  
435 subdomain of 55-kDa tumor necrosis factor receptor. *Virology* **243**:293-302.

436 36. **Doreleijers JF, Langedijk JP, Hard K, Boelens R, Rullmann JA, Schaaper WM, van**  
437 **Oirschot JT, Kaptein R.** 1996. Solution structure of the immunodominant region of protein G of  
438 bovine respiratory syncytial virus. *Biochemistry* **35**:14684-14688.

439 37. **Feldman SA, Hendry RM, Beeler JA.** 1999. Identification of a linear heparin binding domain  
440 for human respiratory syncytial virus attachment glycoprotein G. *J Virol* **73**:6610-6617.

441 38. **Hallak LK, Collins PL, Knudson W, Peeples ME.** 2000. Iduronic acid-containing  
442 glycosaminoglycans on target cells are required for efficient respiratory syncytial virus infection.  
443 *Virology* **271**:264-275.

444 39. **Zhang L, Bukreyev A, Thompson CI, Watson B, Peeples ME, Collins PL, Pickles RJ.** 2005.  
445 Infection of ciliated cells by human parainfluenza virus type 3 in an in vitro model of human  
446 airway epithelium. *J Virol* **79**:1113-1124.

447 40. **Cortjens B, Yasuda E, Yu X, Wagner K, Claassen YB, Bakker AQ, van Woensel JBM,**  
448 **Beaumont T.** 2017. Broadly Reactive Anti-Respiratory Syncytial Virus G Antibodies from  
449 Exposed Individuals Effectively Inhibit Infection of Primary Airway Epithelial Cells. *J Virol* **91**.

450 41. **Lee J, Klenow L, Coyle EM, Golding H, Khurana S.** 2018. Protective antigenic sites in  
451 respiratory syncytial virus G attachment protein outside the central conserved and cysteine noose  
452 domains. *PLoS Pathog* **14**:e1007262.

453 42. **Haynes LM, Caidi H, Radu GU, Miao C, Harcourt JL, Tripp RA, Anderson LJ.** 2009.  
454 Therapeutic monoclonal antibody treatment targeting respiratory syncytial virus (RSV) G protein  
455 mediates viral clearance and reduces the pathogenesis of RSV infection in BALB/c mice. *J Infect*  
456 *Dis* **200**:439-447.

457 43. **Boyoglu-Barnum S, Todd SO, Meng J, Barnum TR, Chirkova T, Haynes LM, Jadhao SJ,**  
458 **Tripp RA, Oomens AG, Moore ML, Anderson LJ.** 2017. Mutating the CX3C motif in the G  
459 protein should make a live respiratory syncytial virus vaccine safer and more effective. *J Virol*  
460 doi:10.1128/JVI.02059-16.

461 44. **Shingai M, Azuma M, Ebihara T, Sasai M, Funami K, Ayata M, Ogura H, Tsutsumi H,**  
462 **Matsumoto M, Seya T.** 2008. Soluble G protein of respiratory syncytial virus inhibits Toll-like  
463 receptor 3/4-mediated IFN-beta induction. *Int Immunol* **20**:1169-1180.

464 45. **Kauvar LM, A Collarini EJ, A Keyt B, A Foord O.** 2010. Anti-RSV G protein antibodies.  
465 **Patent number US 8273354.**

466 46. **Fedechkin SO, George NL, Wolff JT, Kauvar LM, DuBois RM.** 2018. Structures of respiratory  
467 syncytial virus G antigen bound to broadly neutralizing antibodies. *Sci Immunol* **3**.

468 47. **Walsh EE, Falsey AR, Sullender WM.** 1998. Monoclonal antibody neutralization escape  
469 mutants of respiratory syncytial virus with unique alterations in the attachment (G) protein. *J Gen*  
470 *Virol* **79 ( Pt 3)**:479-487.

471 48. **MacRaid CA, Richards JS, Anders RF, Norton RS.** 2016. Antibody Recognition of Disordered  
472 Antigens. *Structure* **24**:148-157.

473 49. **Chu HM, Wright J, Chan YH, Lin CJ, Chang TW, Lim C.** 2014. Two potential therapeutic  
474 antibodies bind to a peptide segment of membrane-bound IgE in different conformations. *Nat*  
475 *Commun* **5**:3139.

476 50. **Yagi M, Bang G, Tougan T, Palacpac NM, Arisue N, Aoshi T, Matsumoto Y, Ishii KJ,**  
477 **Egwang TG, Druilhe P, Horii T.** 2014. Protective epitopes of the *Plasmodium falciparum*

478 SERA5 malaria vaccine reside in intrinsically unstructured N-terminal repetitive sequences. *PLoS*  
479 *One* **9**:e98460.

480 51. **Deng L, Ma L, Virata-Theimer ML, Zhong L, Yan H, Zhao Z, Struble E, Feinstone S, Alter**  
481 **H, Zhang P.** 2014. Discrete conformations of epitope II on the hepatitis C virus E2 protein for  
482 antibody-mediated neutralization and nonneutralization. *Proc Natl Acad Sci U S A* **111**:10690-  
483 10695.

484 52. **Bogdanoff WA, Perez EI, Lopez T, Arias CF, DuBois RM.** 2018. Structural Basis for Escape of  
485 Human Astrovirus from Antibody Neutralization: Broad Implications for Rational Vaccine  
486 Design. *J Virol* **92**.

487 53. **Jones HG, Battles MB, Lin CC, Bianchi S, Corti D, McLellan JS.** 2019. Alternative  
488 conformations of a major antigenic site on RSV F. *PLoS Pathog* **15**:e1007944.

489 54. **McLellan JS, Pancera M, Carrico C, Gorman J, Julien JP, Khayat R, Louder R, Pejchal R,**  
490 **Sastry M, Dai K, O'Dell S, Patel N, Shahzad-ul-Hussan S, Yang Y, Zhang B, Zhou T, Zhu J,**  
491 **Boyington JC, Chuang GY, Diwanji D, Georgiev I, Kwon YD, Lee D, Louder MK, Moquin**  
492 **S, Schmidt SD, Yang ZY, Bonsignori M, Crump JA, Kapiga SH, Sam NE, Haynes BF,**  
493 **Burton DR, Koff WC, Walker LM, Phogat S, Wyatt R, Orwenyo J, Wang LX, Arthos J,**  
494 **Bewley CA, Mascola JR, Nabel GJ, Schief WR, Ward AB, Wilson IA, Kwong PD.** 2011.  
495 Structure of HIV-1 gp120 V1/V2 domain with broadly neutralizing antibody PG9. *Nature*  
496 **480**:336-343.

497 55. **Yuan Y, Cao D, Zhang Y, Ma J, Qi J, Wang Q, Lu G, Wu Y, Yan J, Shi Y, Zhang X, Gao**  
498 **GF.** 2017. Cryo-EM structures of MERS-CoV and SARS-CoV spike glycoproteins reveal the  
499 dynamic receptor binding domains. *Nat Commun* **8**:15092.

500 56. **Kwong PD, Wyatt R, Robinson J, Sweet RW, Sodroski J, Hendrickson WA.** 1998. Structure  
501 of an HIV gp120 envelope glycoprotein in complex with the CD4 receptor and a neutralizing  
502 human antibody. *Nature* **393**:648-659.

503 57. **Escribano-Romero E, Rawling J, Garcia-Barreno B, Melero JA.** 2004. The soluble form of  
504 human respiratory syncytial virus attachment protein differs from the membrane-bound form in its  
505 oligomeric state but is still capable of binding to cell surface proteoglycans. *J Virol* **78**:3524-3532.

506 58. **Fuentes S, Coyle EM, Golding H, Khurana S.** 2015. Nonglycosylated G-Protein Vaccine  
507 Protects against Homologous and Heterologous Respiratory Syncytial Virus (RSV) Challenge,  
508 while Glycosylated G Enhances RSV Lung Pathology and Cytokine Levels. *J Virol* **89**:8193-  
509 8205.

510 59. **Cullen LM, Schmidt MR, Morrison TG.** 2017. The importance of RSV F protein conformation  
511 in VLPs in stimulation of neutralizing antibody titers in mice previously infected with RSV. *Hum*  
512 *Vaccin Immunother* **13**:2814-2823.

513 60. **Krammer F, Pica N, Hai R, Tan GS, Palese P.** 2012. Hemagglutinin Stalk-Reactive Antibodies  
514 Are Boosted following Sequential Infection with Seasonal and Pandemic H1N1 Influenza Virus in  
515 Mice. *J Virol* **86**:10302-10307.

516 61. **Hai R, Krammer F, Tan GS, Pica N, Eggink D, Maamary J, Margine I, Albrecht RA, Palese**  
517 **P.** 2012. Influenza viruses expressing chimeric hemagglutinins: globular head and stalk domains  
518 derived from different subtypes. *J Virol* **86**:5774-5781.

519 62. **Krammer F, Pica N, Hai R, Margine I, Palese P.** 2013. Chimeric hemagglutinin influenza virus  
520 vaccine constructs elicit broadly protective stalk-specific antibodies. *J Virol* **87**:6542-6550.

521 63. **Impagliazzo A, Milder F, Kuipers H, Wagner MV, Zhu X, Hoffman RM, van Meersbergen**  
522 **R, Huizingh J, Wanningen P, Verspuij J, de Man M, Ding Z, Apetri A, Kukrer B, Sneekes-**  
523 **Vriese E, Tomkiewicz D, Laursen NS, Lee PS, Zakrzewska A, Dekking L, Tolboom J,**  
524 **Tettero L, van Meerten S, Yu W, Koudstaal W, Goudsmit J, Ward AB, Meijberg W, Wilson**  
525 **IA, Radosevic K.** 2015. A stable trimeric influenza hemagglutinin stem as a broadly protective  
526 immunogen. *Science* **349**:1301-1306.

527 64. **Lu Y, Welsh JP, Swartz JR.** 2014. Production and stabilization of the trimeric influenza  
528 hemagglutinin stem domain for potentially broadly protective influenza vaccines. *Proc Natl Acad*  
529 *Sci U S A* **111**:125-130.

530 65. **Pallesen J, Wang N, Corbett KS, Wrapp D, Kirchdoerfer RN, Turner HL, Cottrell CA,**  
531 **Becker MM, Wang L, Shi W, Kong WP, Andres EL, Kettenbach AN, Denison MR, Chappell**  
532 **JD, Graham BS, Ward AB, McLellan JS.** 2017. Immunogenicity and structures of a rationally  
533 designed prefusion MERS-CoV spike antigen. *Proc Natl Acad Sci U S A* **114**:E7348-E7357.

66. **Stewart-Jones GBE, Chuang GY, Xu K, Zhou T, Acharya P, Tsybovsky Y, Ou L, Zhang B, Fernandez-Rodriguez B, Gilardi V, Silacci-Fregni C, Beltramello M, Baxa U, Druz A, Kong WP, Thomas PV, Yang Y, Foulds KE, Todd JP, Wei H, Salazar AM, Scorprio DG, Carragher B, Potter CS, Corti D, Mascola JR, Lanzavecchia A, Kwong PD.** 2018. Structure-based design of a quadrivalent fusion glycoprotein vaccine for human parainfluenza virus types 1-4. *Proc Natl Acad Sci U S A* **115**:12265-12270.
67. **McLellan JS, Chen M, Joyce MG, Sastry M, Stewart-Jones GB, Yang Y, Zhang B, Chen L, Srivatsan S, Zheng A, Zhou T, Graepel KW, Kumar A, Moin S, Boyington JC, Chuang GY, Soto C, Baxa U, Bakker AQ, Spits H, Beaumont T, Zheng Z, Xia N, Ko SY, Todd JP, Rao S, Graham BS, Kwong PD.** 2013. Structure-based design of a fusion glycoprotein vaccine for respiratory syncytial virus. *Science* **342**:592-598.
68. **Krarup A, Truan D, Furmanova-Hollenstein P, Bogaert L, Bouchier P, Bisschop IJ, Widjoatmodjo MN, Zahn R, Schuitemaker H, McLellan JS, Langedijk JP.** 2015. A highly stable prefusion RSV F vaccine derived from structural analysis of the fusion mechanism. *Nat Commun* **6**:8143.
69. **Qiao H, Pelletier SL, Hoffman L, Hacker J, Armstrong RT, White JM.** 1998. Specific single or double proline substitutions in the "spring-loaded" coiled-coil region of the influenza hemagglutinin impair or abolish membrane fusion activity. *J Cell Biol* **141**:1335-1347.
70. **Sanders RW, Vesanen M, Schuelke N, Master A, Schiffner L, Kalyanaraman R, Paluch M, Berkhout B, Maddon PJ, Olson WC, Lu M, Moore JP.** 2002. Stabilization of the soluble, cleaved, trimeric form of the envelope glycoprotein complex of human immunodeficiency virus type 1. *J Virol* **76**:8875-8889.
71. **Battles MB, Mas V, Olmedillas E, Cano O, Vazquez M, Rodriguez L, Melero JA, McLellan JS.** 2017. Structure and immunogenicity of pre-fusion-stabilized human metapneumovirus F glycoprotein. *Nat Commun* **8**:1528.
72. **Battye TG, Kontogiannis L, Johnson O, Powell HR, Leslie AG.** 2011. iMOSFLM: a new graphical interface for diffraction-image processing with MOSFLM. *Acta Crystallogr D Biol Crystallogr* **67**:271-281.
73. **Evans PR, Murshudov GN.** 2013. How good are my data and what is the resolution? *Acta Crystallogr D Biol Crystallogr* **69**:1204-1214.
74. **McCoy AJ, Grosse-Kunstleve RW, Adams PD, Winn MD, Storoni LC, Read RJ.** 2007. Phaser crystallographic software. *J Appl Crystallogr* **40**:658-674.
75. **Adams PD, Afonine PV, Bunkoczi G, Chen VB, Davis IW, Echols N, Headd JJ, Hung LW, Kapral GJ, Grosse-Kunstleve RW, McCoy AJ, Moriarty NW, Oeffner R, Read RJ, Richardson DC, Richardson JS, Terwilliger TC, Zwart PH.** 2010. PHENIX: a comprehensive Python-based system for macromolecular structure solution. *Acta Crystallogr D Biol Crystallogr* **66**:213-221.
76. **Emsley P, Cowtan K.** 2004. Coot: model-building tools for molecular graphics. *Acta Crystallogr D Biol Crystallogr* **60**:2126-2132.

## FIGURE LEGENDS

**Fig. 1.** Crystal structure of the Fab 3G12-RSV G<sup>157-197</sup> complex. (A) Schematic of the RSV G glycoprotein from RSV strain A2, including the transmembrane region (TM), CCD, and the cysteine noose (Cys noose). Met48 is the alternate initiation site for the production of soluble RSV G. Predicted N- and O-linked glycans are shown by red “Y” and blue “O,” respectively. Below is a sequence logo of residues 160-197 of the RSV G CCD, revealing the sequence conservation across strains RSV A, RSV B, RSV L, and RSV 1-8. (B) Overall views of antibody 3G12 heavy chain (dark grey) and light chain (light grey) bound to RSV G<sup>157-197</sup> (cyan, with disulfides in yellow). (C) Detailed views of interactions between antibody 3G12 with RSV G CCD, with the same viewpoints as in panel B. Hydrogen bonds are shown as dashes. Heavy-chain CDRs (HCDR1-3) and light-chain CDRs (LCDR1 and 3) are labeled.

**Fig. 2.** Comparison of known RSV G CCD epitopes and structures. Epitope amino acids interacting with antibodies are colored as follows: 3G12 (blue), CB002.5 (gold), 3D3 (green), CB017.5 (magenta), and 2D10 (cyan). Bottom panels are rotated 180 degrees around the y-axis compared to top panels. Epitope amino acids were determined by the PDBePISA server and are written below each structure.

**Fig. 3.** Differences in bnmAb 3G12 and bnmAb 3D3 binding to RSV G<sup>ecto</sup> F170P. (A) Coomassie-stained SDS-polyacrylamide gel of RSV G<sup>ecto</sup> (Wild-Type) and RSV G<sup>ecto</sup> F170P (F170P). Molecular weight (MW) ladder values are labeled in kilodaltons. (B) Structure of RSV G CCD when bound to bnmAb 3D3 (top) and bnmAb 3G12 (bottom).

F170 is colored red. (C) Biolayer interferometry traces (blue) and curve fits (red) for binding of bnmAb 3D3 (top) and bnmAb 3G12 (bottom) to RSV  $G^{ecto}$  and RSV  $G^{ecto}$  F170P. Concentrations of  $G^{ecto}$  used for each trace are shown. The vertical red line indicates the transition of the biosensors from the association step to the dissociation step. Binding on-rates, off-rates, dissociation constants, and curve fit statistics are shown in Table 2.

**Fig. 4.** Proposed model relating antigenic site flexibility, antibody response diversity to that site, and potential for virus neutralization escape at that site.

609 **Table 1. Crystallographic data collection and refinement statistics**  
610

	<b>Fab 3G12-RSV G<sup>157-197</sup></b>
PDB code	6UVO
<b>Data collection<sup>a,b</sup></b>	
Space group	<i>P</i> 3 <sub>1</sub> 21
Cell dimensions	
<i>a</i> , <i>b</i> , <i>c</i> (Å)	139.33 139.33 94.77
$\alpha$ , $\beta$ , $\gamma$ (°)	90, 90, 120
Resolution (Å)	74.53 - 2.90 (3.00 - 2.90)
Total no. reflections	93,208 (14,475)
No. unique reflections	23,682 (3,763)
<i>R</i> <sub>merge</sub> <sup>c</sup>	0.097 (0.641)
<i>I</i> / $\sigma$ ( <i>I</i> )	9.4 (1.9)
Completeness (%)	99.5 (99.5)
Redundancy	3.9 (3.8)
CC <sub>1/2</sub> <sup>d</sup>	0.993 (0.601)
<b>Refinement</b>	
Resolution (Å)	74.53 - 2.90
No. reflections	23,665
<i>R</i> <sub>work</sub> / <i>R</i> <sub>free</sub> <sup>e</sup>	0.193/ 0.209
No. atoms	
Protein	3,595
Ligand/ion	0
Water	0
<i>B</i> -factors (Å <sup>2</sup> )	
Protein: bnmAb	62
Protein: RSV G	76
Ligand/ion	0
R.m.s. deviations	
Bond lengths (Å)	0.015
Bond angles (°)	2.067
Ramachandran (%)	
Favored	95.7
Allowed	4.3
Outliers	0

611 <sup>a</sup> Data from one crystal was used.

612 <sup>b</sup> Values in parentheses are for highest-resolution shell.

613 <sup>c</sup> *R*<sub>merge</sub> =  $\Sigma|I - \langle I \rangle| / \Sigma(I)$ , where *I* is the observed intensity.

614 <sup>d</sup> CC<sub>1/2</sub> = Pearson correlation coefficient between random half-datasets.

615 <sup>e</sup> *R*<sub>work</sub> =  $\Sigma||F_o| - |F_c|| / \Sigma|F_o|$  for all data except 5%, which were used for *R*<sub>free</sub> calculation

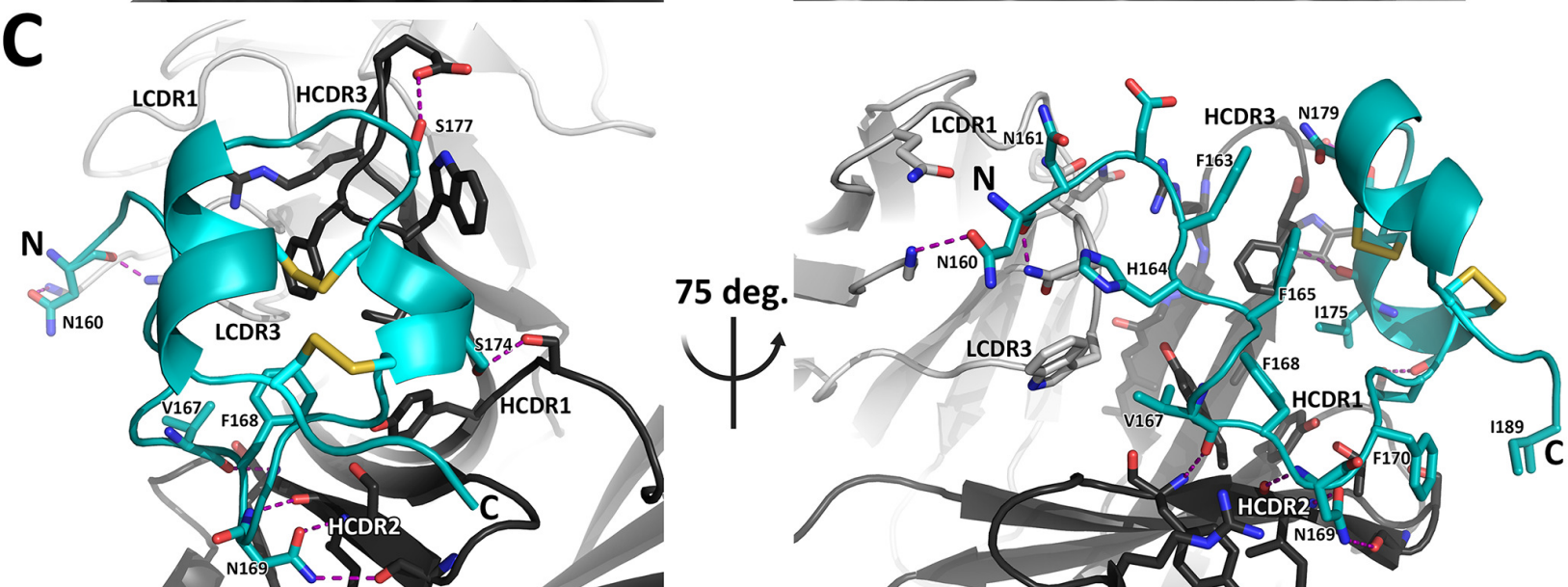
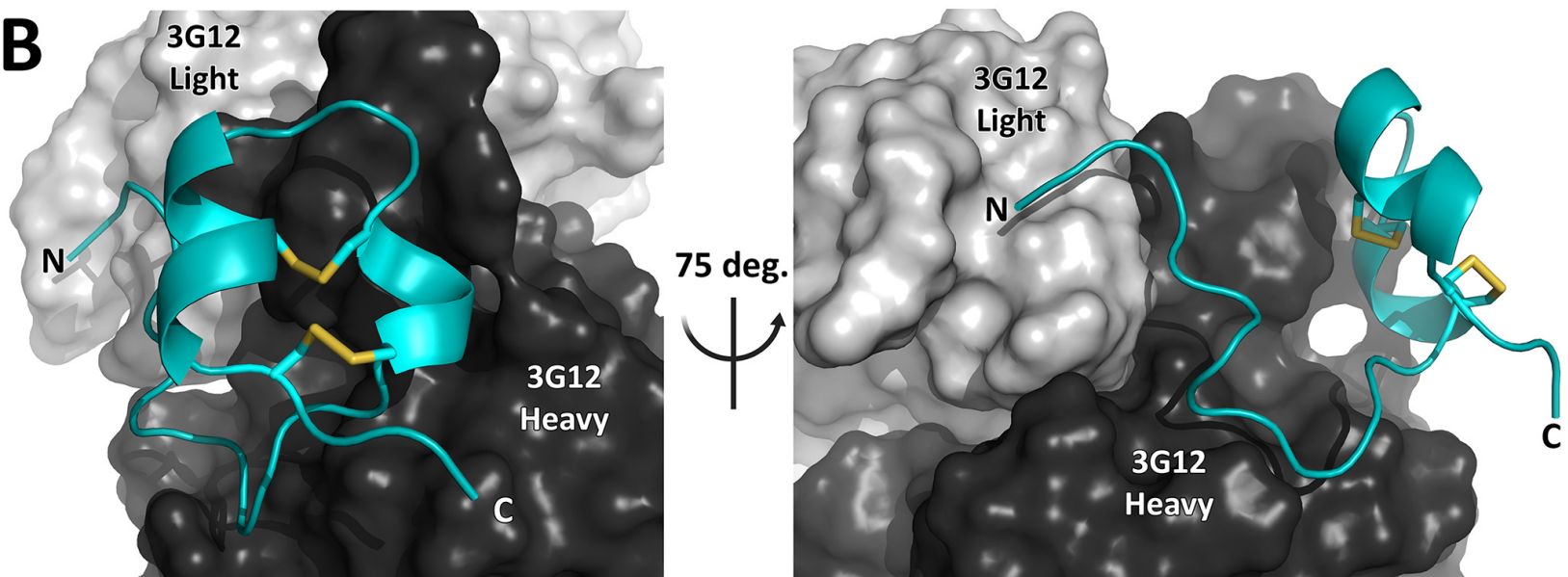
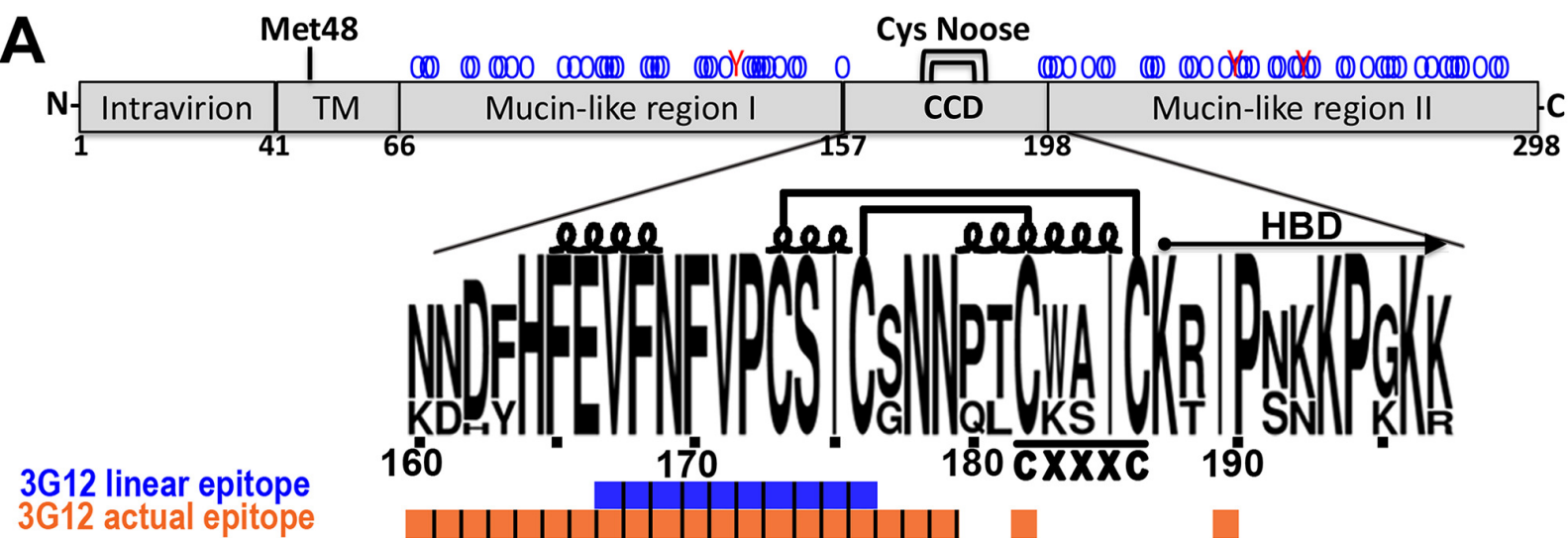
616

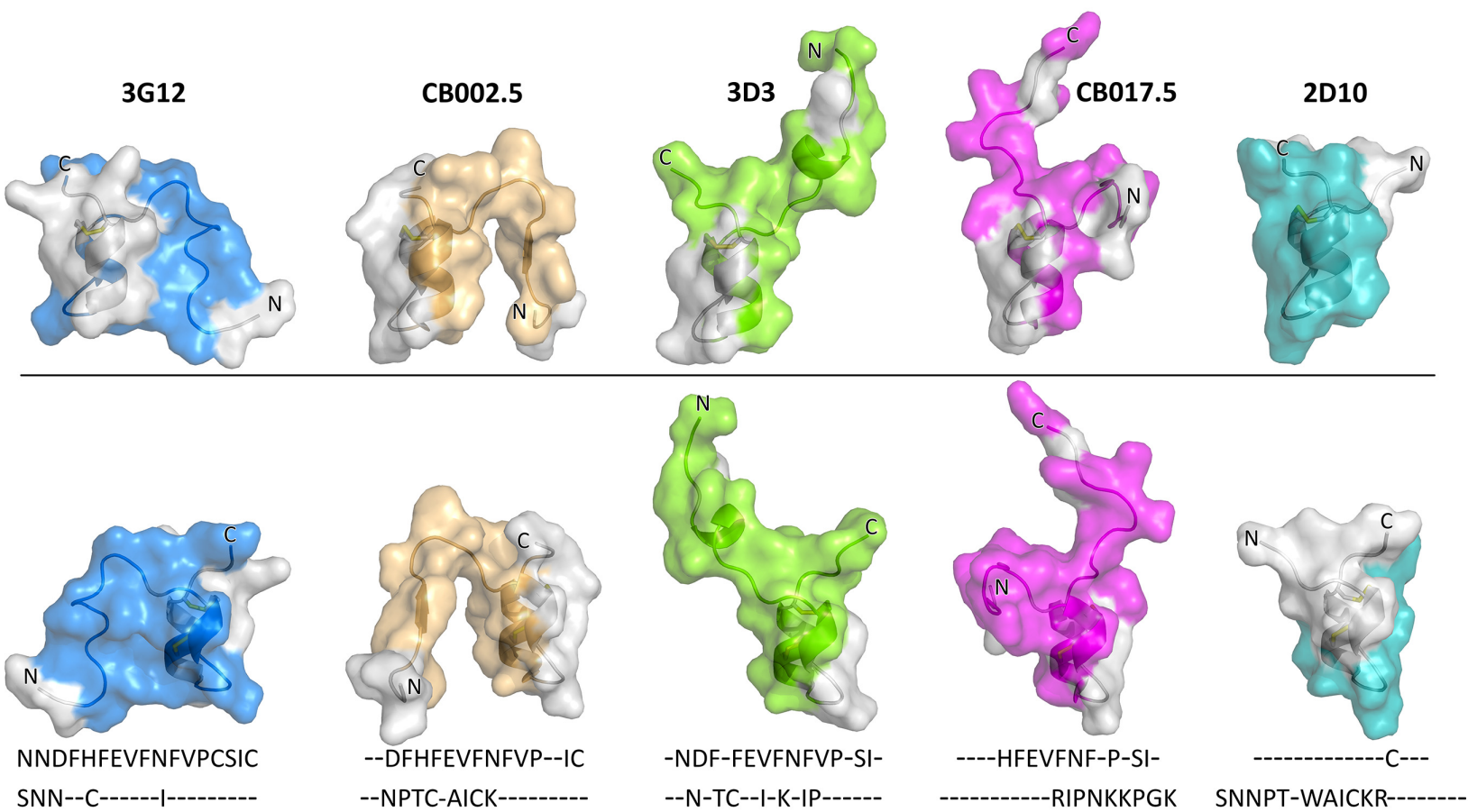


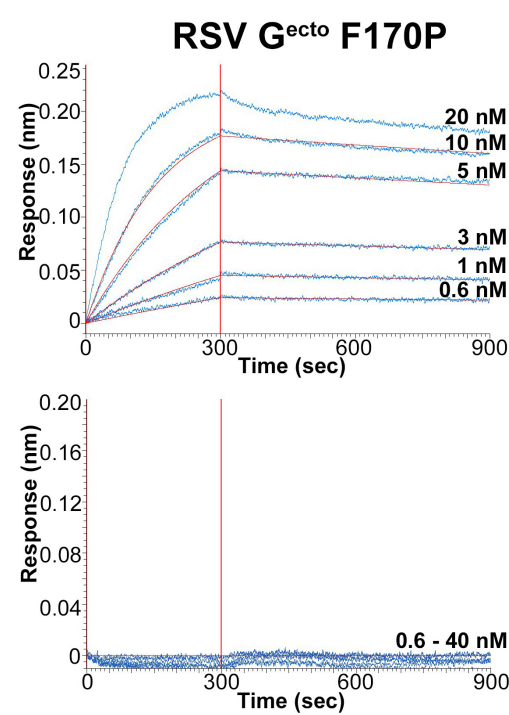
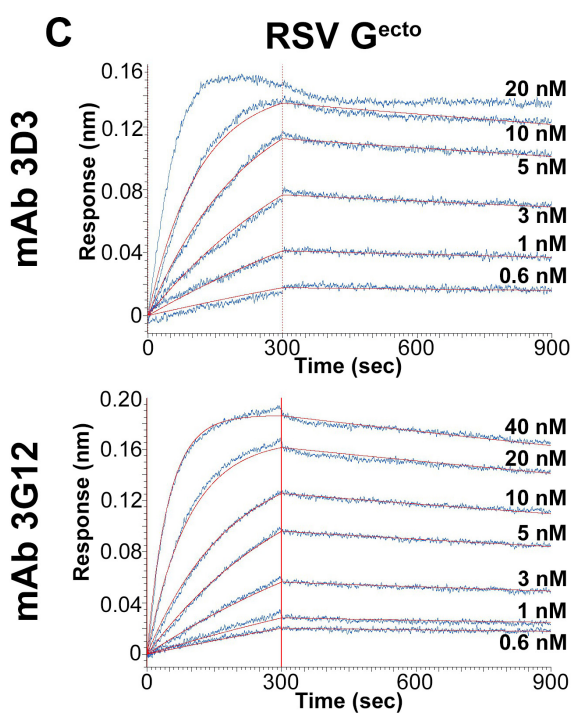
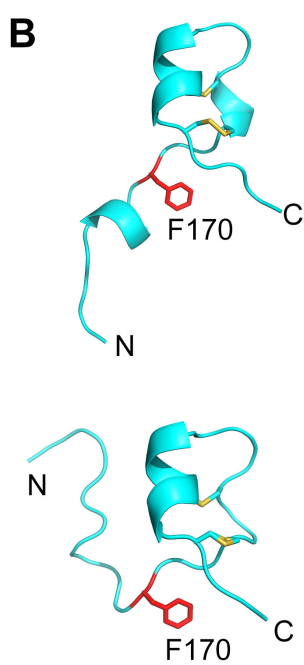
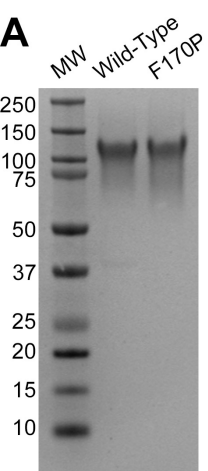
**Table 2. Biolayer interferometry binding studies<sup>a</sup>**

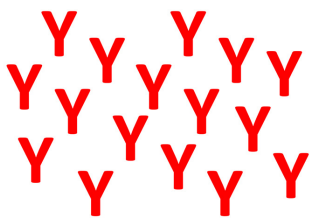
Sample	bnmAb	$K_D$ (pM)	$k_a$ ( $\times 10^5 \text{ M}^{-1} \text{ s}^{-1}$ )	$k_d$ ( $\times 10^{-4} \text{ s}^{-1}$ )	$R^2$
RSV G <sup>ecto</sup>	3D3	202 ( $\pm 1$ )	8.73 ( $\pm 0.02$ )	1.77 ( $\pm 0.01$ )	0.998
RSV G <sup>ecto</sup> F170P	3D3	264 ( $\pm 1$ )	6.23 ( $\pm 0.01$ )	1.65 ( $\pm 0.01$ )	0.999
RSV G <sup>ecto</sup>	3G12	423 ( $\pm 1$ )	5.27 ( $\pm 0.01$ )	2.23 ( $\pm 0.01$ )	0.999
RSV G <sup>ecto</sup> F170P	3G12	N.B. <sup>a</sup>	-	-	-

<sup>a</sup>  $K_D$ , binding dissociation constant.  $k_a$ , on-rate.  $k_d$ , off-rate.  $R^2$ , curve fit statistic. N.B., no binding observed. Values in parentheses are the standard error.



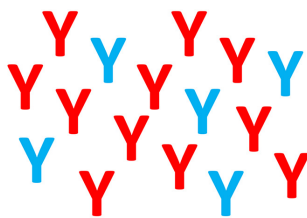






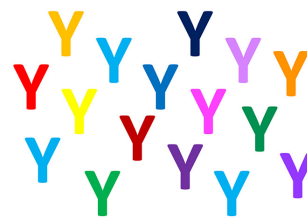
**No diversity**

**Monoclonal antibody**



**Low diversity**

**Polyclonal antibody**



**High diversity**

**Polyclonal antibody**

**Antigenic site flexibility**

**Potential for virus neutralization escape**